The strengths of scanning electron microscopy in deciphering SARS-CoV-2 infectious cycle

Short title (for the running head): The infectious cycle of SARS-CoV-2 (COVID-19)

Article type: original research

Author list: Djamal Brahim Belhaouari[1], Anthony Fontanini[2], Jean-Pierre Baudoin[1] , Gabriel Haddad[1], Marion Le Bideau[1], Jacques Yaacoub Bou Khalil[2], Didier Raoult[1], Bernard La Scola[1,2*]

Affiliations:

[1]Microbes, Evolution, Phylogeny and Infection (MEPHI), UM63, Institut de Recherche pour le Développement (IRD), Assistance Publique - Hôpitaux de Marseille (AP-HM), Aix-Marseille University, Marseille, France.

[2]IHU Méditerranée Infection, Marseille, France

*** Corresponding author:** Pr Bernard La Scola, Microbes, Evolution, Phylogeny and Infection (MEPHI), UM63, Institut de Recherche pour le Développement (IRD), IHU Méditerranée Infection, Assistance Publique - Hôpitaux de Marseille (AP-HM), Aix-Marseille University, 19-21 boulevard Jean Moulin, 13005 Marseille, France.

Email : **bernard.la-scola@univ-amu.fr**

Abstract

Electron microscopy is a powerful tool in the field of microbiology. It has played a key role in the rapid diagnosis of viruses in patient samples and has contributed significantly to the clarification of virus structure and function, helping to guide the public health response to emerging viral infections. In the present study, we used scanning electron microscopy (SEM) to study the infectious cycle of SARS-CoV-2 (COVID-19) in Vero E6 cells and we controlled some key findings by classical transmission electronic microscopy (TEM). The replication cycle of the virus was followed from 1 to 52 hours post-infection. Our results revealed that SARS-CoV-2infected the cells through membrane fusion. Particles are formed in the peri-nuclear region from a budding of the endoplasmic reticulum - Golgi apparatus complex into morphogenesis matrix vesicae. New SARS-CoV-2 particles were expelled from the cells, through cell lysis or by fusion of virus-containing vacuoles with the cell plasma membrane. Overall, this cycle is highly comparable to that of SARS-CoV. By providing a detailed and complete SARS-CoV-2 infectious cycle, SEM proves to be a very rapid and efficient tool compared to classical TEM.

Key words: SARS CoV-2, infectious cycle, Vero E6 cells, scanning electron microscopy (SEM).

Introduction

The SARS-CoV-2 (COVID-19) outbreak started in late December 2019 in China and has since reached a global pandemic (Zhu et al., 2020), leading to a worldwide battle against COVID-19. SARS-CoV-2 is a novel β-coronavirus belonging to the sarbecovirus subgenus of Coronaviridae family (Schoeman and Fielding, 2019; Zhu et al., 2020). Coronaviruses are enveloped viruses with a positive sense, single-stranded RNA genome (Schoeman and Fielding, 2019). One of the first methods used is Electron Microscopy (EM), which has been a reliable tool for the classification of viruses according to their ultra-structure (Curry et al., 2006; Hazelton and Gelderblom, 2003)The characteristic morphology of crown-like structures detected by EM explains the name of *Coronaviridae* family (Golding et al., 2016) observed as widely spaced club-shaped projections surrounding the virus envelope, thus forming a crown aspect in negative staining protocols (Almeida and Tyrrell, 1967; Oshiro et al., 1971). Coronaviruses have the largest genomes among RNA viruses, with genome sizes ranging from 26 to 32 kilobases (kb) in length. These viruses primarily infect birds and mammals, and can also infect humans, causing respiratory and enteric diseases, such as upper respiratory tract infections and lower respiratory tract infections (bronchitis, pneumonia, and severe acute respiratory syndrome (SARS). Coronaviruses have caused three worldwide pandemics associated with SARS in the past two decades, including SARS-CoV in 2003, Middle East Respiratory Syndrome – Coronavirus (MERS-CoV) in 2012 and the present SARS-CoV-2.

Electron microscopy (EM) is a powerful tool in the field of microbiology, because of its resolution power as compared to light microscopy (Koster and Klumperman, 2003). EM contributed significantly to the clarification of viruses structure and function and has played a key role in the rapid diagnosis of viruses in various samples (Goldsmith and Miller, 2009). The ability of EM to detect unknown and unsuspected organisms has made it a suitable tool to guide the public health response during previous outbreaks. Transmission electron microscopy (TEM) was extensively

used to describe the morphology or the morphogenesis of SARS-CoV (Ng et al., 2003; Qinfen et al., 2004), MERS-CoV (Alsaad et al., 2018; Kim et al., 2016; Park et al., 2016) or, more recently, SARS-CoV-2 (Caly et al., 2020; Colson et al., 2020; Kim et al., 2016; Park et al., 2016; Zhu et al., 2020).

Scanning electron microscopy (SEM) is another powerful tool for microbiological research and diagnosis of infectious diseases (Golding et al., 2016). We already demonstrated its strengths for ultra-rapid microscope imaging of SARS-CoV-2 when pandemic first reached France (Colson et al., 2020). Here, we used SEM for its capacity to rapidly screen SARS-CoV-2-infected Vero cells in resin ultra-thin sections, allowing the ultrastructural detailed analysis of SARS-CoV-2 throughout the whole infectious cycle.

Material and methods

Cell culture-virus infectious cycle

Vero E6 cells were grown as a monolayer in 25 cm^2 culture flasks in Dulbecco′s Modified Eagle′s Medium supplemented with 10% fetal bovine serum for two to three days at 37°C. For the viral infectious cycle, the culture medium was removed and the cells were inoculated with SARS-CoV-2. After incubation at 37°C for one hour, the supernatant was then removed and the cultures were gently rinsed three times with culture media to eliminate any excess of viral particles, marking time 0 (H0). For later time points, the infected and rinsed cells were incubated at 37°C in culture medium. Hourly post-infection time points were: H1, H2, H3, H4, H5, H6, H12, H24, H36, H48 and H52. For each time point, the infected cells were detached using 500µl of trypsin and pelleted by centrifugation at 500×g for 10 minutes.

Scanning and Transmission Electron Microscopy

For electron microscopy infected Vero cells were fixed at least for one hour with glutaraldehyde 2.5% in 0.1M sodium cacodylate buffer. For resin embedding, cells were washed three times with a mixture of 0.2M saccharose/0.1M sodium cacodylate. Cells were post-fixed for one hour with 1% OsO_4 diluted in 0.2M Potassium hexa-cyanoferrate (III) / 0.1M sodium cacodylate solution. After three 10-minute washes with distilled water, the cells were gradually dehydrated with ethanol by successive 10-minute baths in 30%, 50%, 70%, 96%, 100% and 100% ethanol. Substitution was achieved by successively placing the cells in 25%, 50% and 75% Epon solutions for 15 minutes. Cells were placed for one hour in 100% Epon solution and in fresh Epon 100% over-night under vacuum at room-temperature. Polymerization occured with cells in 100% fresh Epon for 72 hours at 60°C. All solutions used above were 0.2µm filtered. Ultrathin 70 nm sections were cut using a UC7 ultramicrotome (Leica) and placed on HR25 300 Mesh Copper/Rhodium grids (TAAB, UK). Sections were contrasted according to Reynolds (Reynolds, 1963). For scanning electron microscopy (SEM), sections on grids were platinum-coated with a MC1000 sputter coater (Hitachi) for 40seconds at 10mA. Electron micrographs were obtained on either SU5000 SEM (Hitachi High-Tech, HHT, Japan) operated between 7 kV and 10 kV accelerating voltage, in high-vacuum and observation mode (spot size 30), between 4.6 mm and 4.9 mm average working distance with BSE detector, and magnifications ranging from x5,000 to x100,000 or Tecnai G^2 TEM (Thermo-Fischer/FEI) operated at 200 keV equipped with a 4096 x 4096 pixels resolution Eagle camera (FEI).

Results

SARS-CoV-2 cell entry

At very early post-infection time-points, from H0 to H5, SARS-CoV-2 virions were not detected in the ultra-thin sections. From H6 further, viral particles could be detected by SEM and TEM at the surface of the cells, mostly at their apical side at the microvilli level (Figure1). From H6

to H12, most of the viruses attached to cell plasma membranes were seen in cells that were not replicating new virions. In those cells, probably in the process of being infected, no virus-proliferation status was observed (see below). However, viruses attached to the plasma membrane were located at the periphery of virus-producing cells starting H12, where viral particles at the surface were located between microvilli, at the level of a smooth plasma membrane or in cellular invaginations. When located on the plasma membrane of non-productive cells, particles were seen i) attached, with their corona spikes located between the particle and the plasma membrane (Figure1.A,B) or ii) less electron-dense, with the capsid fusing with the plasma membrane (Figure1.C-E). The formation of endocytic vesicles with typical clathrin-coated pits was often observed when the particles were attached to the plasma membrane (Figure2.A-F). In these forming endocytic particles, rod-like amorphous material was present (Figure 2). This kind of material was also observed in clathrin-coated endocytic vesicles located more deeply in the cell cytoplasm (Figure 2.G,H). We also observed in the cytoplasm of the non-producing cells electron-dense crescent-shaped intracellular structures (Figure2.A,B) that were also present in control, non-infected cells. Inside non-producing cells, a very few virus-like particles were observed inside the cells in endoplasmic reticulum (ER)-derived peripheral canaliculi. From H24 onwards, most of the viruses attached to cell plasma membranes were seen in intact- or lysed- virus producing-cells.

SARS-CoV-2 morphogenesis

At the nucleus level, round empty particles and round particles with a punctate pattern at their center were observed at nucleus margins (Figure 3.A-F). These nascent particles were seen at locations where the nuclear membrane was not clearly delineated, in contrast to adjacent nuclear regions where the double membrane was properly seen. These nuclear membrane budding sites could be observed in transverse (Figure 3.A-E,G) or in tangential views (Figure 3.F,H), the particles being, in the latter case, located in an electron-dense chromatin-like material, which we called

nuclear matrix. The mean diameter of these particles ranged from 80 nm to 112 nm as measured by SEM and TEM (Figure 3.C-F).

Swollen nuclear membrane, endoplasmic reticulum (ER) and Golgi apparatus (GA) organelles were the most striking features of SARS-CoV-2 infected cells (Figure 4). Thick and distorted ER tubules were observed at peri-nuclear locations between the nucleus and the GA (Figure 4.A,B), and also at peripheral locations below the plasma membrane, where the ER could be seen as zippered (Figure 4.G). When intact, the GA was found at peri-nuclear locations, with Golgi stacks lying parallel to the ER and the nuclear membranes (Figure 4.A,B). As infection progressed, the GA was found budding between large ER tubules, resulting in multiple Golgi-derived nascent particles and a loss of intact GA stacks (Figure 4.D-F). The extent of GA budding was variable from a cell to another, being generally proportional to its distance from the nucleus. At early infection stages, myelin-like membranes whorls were observed at proximity of the Golgi apparatus (Figure 4.C). These whorl types are probably not a typical feature of infected cells, as they have also been observed in uninfected cells. We also noticed abundant mitochondria in apical regions of both non-infected and infected cells at all stages, around the ER and Golgi-rich regions.

Golgi-derived doughnut-like particles with a pronounced electron-opaque edge were observed at peri-nuclear locations (Figure 5.A,B), dispersed into the cytoplasm, as well as entering vacuoles, which seemed to be derived from the ER (Figure 5.A,B). Such forming virus morphogenesis matrix vesicae (Qinfen et al., 2004), filled with doughnut-like particles, were observed as open sacs, assembling next to the nucleus (Figure 5.A,B), or closed sacs adjacent to or distant from the nucleus, in the cytoplasm or in the vacuoles (Figure 5.C,D). Doughnut-like particles were devoid of corona spikes. Their shape was not perfectly round when observed in the assembling opened sacs, which could present a filopodia-like protrusion (Figure 5.B).

As the infection progressed, we observed an extensive network of membrane whorls, with large inter-membranous distances when compared to previous 'small' membrane whorls (Figure 6.A). These intermingled membranes were lying at the level of concave nuclear indentations. Nascent virions could be found mixed with such membranes whorls in large bags (Figure 6.B). The appearance of the virus morphogenesis matrix vesicae (VMMV) was variable, with nascent particles located in more or less large vacuoles, containing more or less electron-dense material (Figure.6 C-F). The electron-density of these vacuoles filled with nascent particles was correlated with the heterogeneity of these vacuoles: electron-dense virions-filled vacuoles were homogenous (Figure 6.C,D), while electron-lucent vacuoles contained virions particles as well as heterogeneous materials such as membranes, or distorted compartments (Figure 6.E,F). VMMV located below the plasma membrane were frequently seen translucent, with well-individualized virions particles (Figure 6.F). We also noticed that particles could arrange as circular chains lying on the internal surface of the VMMV (Figure 6.D).

SARS-CoV-2 cell exit

Mature SARS-CoV-2 particles were observed as spiky round to hexagonal electron-dense particles (Figure7,8). Mature SARS-CoV-2 particles were observed at extra- and intra-cellular locations: in translucent VMMV or vacuoles of early infected intact cells (Figure 6.E, 7), and later found lying between cellular microvilli (Figure 8.A-C), in vacuoles (Figure 8.G), as well as on the surface (Figure 8.F,H) of lysed cells. Intracellular compartments filled with mature virions (Figure 7,8) were observed channeling with the apical side of the Vero cells at the base of the microvilli (Figure 8.C,E).

Discussion

Our results show spiky round to hexagonal 80 to 112 nm in diameter electron-dense mature SARS-CoV-2 particles, similar to the previously described SARS-CoV-2 virions (Colson et al., 2020; Kim et al., 2020; Park et al., 2016; Zhu et al., 2020). Previous analysis of ultrathin sections by TEM of SARS-CoV-2 infected- cells showed virus particles in inclusion bodies in human airway cells (Zhu et al., 2020), as well as in a wide range of intracellular organelles, especially in vesicles of Vero cells (Caly et al., 2020; Kim et al., 2020; Park et al., 2016). Here, thanks to our SEM analysis, we were able to show the similarity between SARS-CoV-2 and SARS-CoV infectious cycles, with some exceptions. Our non-observation at very early post-infection time-points of SARS-CoV-2 virions in the ultra-thin sections is probably related to the very brief binding of infectious particles to the cell surface, and the rapid reduction of the particle once attached to the cells. From H6 further, it cannot be ruled out that the particles on the cell surface are neo-synthesized virions produced by infected cells.

Regarding SARS-CoV-2 cell entry process, particles were observed attached at cells plasma membrane similarly to SARS-CoV, located at cells apical sides (Rossen et al., 1994). Full SARS-CoV-2 particle endocytosis was not observed, which is consistent with previous studies conducted on SARS-CoV particles infecting cells by membrane fusion (Ng et al., 2003; Oshiro et al., 1971; Qinfen et al., 2004). In fact, we observed a possible fusion of SARS-CoV-2 particles with the cells plasma membranes. Our images suggest that these attached particles were probably caught transferring their content inside the cell cytoplasm. Crescent-shaped intracellular structures, also observed in non-infected cells, might actually correspond either to virions remnants after fusion of the particles with the plasma membrane, or to clathrin-coated vesicle after their uncoating and opening inside the cytoplasm. The role of the clathrin endocytic vesicles containing amorphous material, as intermediate receptacles of SARS-CoV-2 genomic content after fusion of the particles with cells plasma membranes, is likely to be part of the SARS-CoV-2 nucleocapsid cell entry process.

Regarding SARS-CoV-2 morphogenesis, previous studies reported nuclear localization of SARS-CoV proteins or particles (Qinfen et al., 2004; Yuan et al., 2005; Zhang et al., 2003). Here, we did not observe intact particles inside the nucleus, but rather nascent particles in a nuclear matrix without a distinctive membranous limit. The abundance of mitochondria next to the ER and GA budding regions, where SARS-CoV-2 morphogenesis occurred, could provide energy for viral multiplication (Castro et al., 2013). It was assumed that doughnut-shaped electron-dense structures (also observed in SARS-CoV infectious cycle studies) probably correspond to assemblies of virus genomes together with helical nucleocapsids (Ng et al., 2003). As in SARS-CoV-2 infected cells, myelin-like membrane whorls have been previously described in SARS-CoV infected cells, closely associated with nascent particles (Ng et al., 2003). We hypothesize that these membrane whorls may be derived from the ER or may be part of an auto-phago-(lyso)somal process, both scenarios providing a support for virions packaging and trafficking until further extracellular release. The electron-density and homogeneity difference of the VMMV containing viral particles may be related to the pH of these compartments and/or to the maturation level of the virions. The circular aspect of SARS-CoV-2 assemblies inside some VMMVs may reflect the presence of mature particles, compared to immature and dispersed particles in less organized VMMV. As for SARS-CoV infected cells, one of the most obvious ultrastructural changes in SARS-CoV-2 infected cells is the proliferation of the Golgi complexes and related vesicles, accompanied by swelling of some of the Golgi sacs. We also found that VMMVs are most probably derived from the ER. It was shown that SARS-CoV nucleocapsids assemble in the ER and mature by budding into smooth vesicles derived from the GA. In parallel, the GA swells to form smooth vesicles that incorporate the VMMV along with their nucleocapsids (Oshiro et al., 1971; Patterson and Macnaughton, 1982; Qinfen et al., 2004; Siu et al., 2008; Zhang et al., 2003). Rather, our images suggest that nascent particles may bud in the cytoplasm, followed or simultaneous to the filling of the ER-derived VMMV by immature Golgi-derived virions. Nevertheless, the involvement of the Endoplasmic

Reticulum - Golgi Apparatus complex witnessed here, especially the extreme budding of the Golgi apparatus, into the morphogenesis of the SARS-CoV-2, is consistent with the demonstrated efficacy of chloroquine, a pharmacological inhibitor, which interferes with cell trafficking by lowering the pH of intracellular compartments (Devaux et al., 2020).

Regarding SARS-CoV-2 cell exit, mature virions exited the cells at their apical sides, as observed for SARS-CoV (Rossen et al., 1994). The release of mature particles occurred passively in lysed cells or by fusion of the internal compartments with the plasma membrane in intact cells, as previously described (Ng et al., 2003; Oshiro et al., 1971; Qinfen et al., 2004).

Scanning electron microscopy (SEM) has shown several advantages over transmission electron microscopy (TEM) for studying SARS-CoV-2 life cycle. First, it was possible to load multiple ultra-thin sections of resin-embedded infected cells, fixed at different time points post-infection and loaded onto carbon grids that were applied onto one glass slide for simultaneous observation and instant comparison after a single vacuum. All conditions were accessible within 10 minutes. Once the beam axis alignment performed, screening of the ultra-thin sections was fast, as only minor adjustments of the focus distance over large regions were needed. The whole SARS-CoV-2 life cycle was thus accessible at once, in a few hours of observation (4.5 hours for 8 time-points, acquiring 320 micrographs), with possibilities to image at the cell population, cellular and sub-cellular levels. Secondly, the balance between the high-resolution micrographs and the speed and ease of screening large cell numbers, at different scales, in different conditions made it possible to rapidly detect individual SARS-CoV-2 particles and precisely study its morphogenesis and infectious cycle.

In conclusion, SEM has proven to be a rapid and effective tool for studying the SARS-CoV-2 infectious cycle in Vero cells. Further studies employing the same straightforward methodology may help understand at the cellular level the impact of pharmacological reagents on SARS-CoV-2 life cycle to better control this global pandemic.

Author Contributions

D-BB, J-PB, GH, MB, AF and JBK did the experiments and analyzed the data. D-BB, J-PB, GH wrote the manuscript. J-PB , JBK, DR and BL conceived the project, supervised the experiments, and wrote the manuscript.

Funding

This work was supported by the French Government under the "Investments for the Future" programme managed by the National Agency for Research (ANR), Méditerranée-Infection 10-IAHU-03 and was also supported by Région Provence-Alpes-Côte d'Azur and European funding FEDER PRIMMI (Fonds Européen de Développement Régional - Plateformes de Recherche et d'Innovation Mutualisées Méditerranée Infection). In addition, collaborative study conducted by IHU Méditerranée Infection and the Hitachi High-Tech Corporation is funded by the Hitachi High-Tech Corporation.

Conflict of Interest

Authors would like to declare that Didier Raoult is a consultant for the Hitachi High-Tech Corporation. Funding sources had no role in the design and conduct of the study, the collection, management, analysis and interpretation of the data, nor in the preparation, review or approval of the manuscript.

Acknowledgments

We sincerely thank Rita Jaafar, Isabelle Duflot and Julien Andreani for their technical help. We also thank Takashi Irie, Kyoko Imai, Shigeki Matsubara, Taku Sakazume, Toshihide Agemura, Yusuke Ominami and the Hitachi team in Japan from Hitachi High-Tech Corporation and Hitachi Ltd. for the collaborative study conducted together with IHU Méditerranée Infection, and for the installation of a SU5000 microscope at the IHU Méditerranée Infection facility.

References

Almeida, J.D., and Tyrrell, D.A. (1967). The morphology of three previously uncharacterized human respiratory viruses that grow in organ culture. J. Gen. Virol. *1*, 175–178. doi:10.1099/0022-1317-1-2-175

Alsaad, K.O., Hajeer, A.H., Al Balwi, M., Al Moaiqel, M., Al Oudah, N., Al Ajlan, A., AlJohani, S., Alsolamy, S., Gmati, G.E., Balkhy, H., et al. (2018). Histopathology of Middle East respiratory syndrome coronovirus (MERS-CoV) infection - clinicopathological and ultrastructural study. Histopathology *72*, 516–524.doi:10.1111/his.13379

Caly, L., Druce, J., Roberts, J., Bond, K., Tran, T., Kostecki, R., Yoga, Y., Naughton, W., Taiaroa, G., Seemann, T., et al. (2020). Isolation and rapid sharing of the 2019 novel coronavirus (SARS-CoV-2) from the first patient diagnosed with COVID-19 in Australia. Med. J. Aust.doi: 10.5694/mja2.50569

Castro, I.F. de, Volonté, L., and Risco, C. (2013). Virus factories: biogenesis and structural design. Cellular Microbiology *15*, 24–34.doi:10.1111/cmi.12029

Colson, P., Lagier, J.-C., Baudoin, J.-P., Bou Khalil, J., La Scola, B., and Raoult, D. (2020). Ultrarapid diagnosis, microscope imaging, genome sequencing, and culture isolation of SARS-CoV-2. Eur. J. Clin. Microbiol. Infect. Dis.doi:10.1007/s10096-020-03869-w

Curry, A., Appleton, H., and Dowsett, B. (2006). Application of transmission electron microscopy to the clinical study of viral and bacterial infections: Present and future. Micron *37*, 91–106.doi: 10.1016/j.micron.2005.10.001

Devaux, C.A., Rolain, J.-M., Colson, P., and Raoult, D. (2020). New insights on the antiviral effects of chloroquine against coronavirus: what to expect for COVID-19? Int. J. Antimicrob. Agents 105938.doi:10.1016/j.ijantimicag.2020.105938

Golding, C.G., Lamboo, L.L., Beniac, D.R., and Booth, T.F. (2016). The scanning electron microscope in microbiology and diagnosis of infectious disease. Sci Rep *6*, 26516.doi: 10.1038/srep26516

Goldsmith, C.S., and Miller, S.E. (2009). Modern uses of electron microscopy for detection of viruses. Clinical Microbiology Reviews.doi:10.1128/CMR.00027-09

Hazelton, P.R., and Gelderblom, H.R. (2003). Electron microscopy for rapid diagnosis of infectious agents in emergent situations. Emerging Infectious Diseases.doi: 10.3201/eid0903.020327

Kim, J.-M., Chung, Y.-S., Jo, H.J., Lee, N.-J., Kim, M.S., Woo, S.H., Park, S., Kim, J.W., Kim, H.M., and Han, M.-G. (2020). Identification of Coronavirus Isolated from a Patient in Korea with COVID-19. Osong Public Health Res Perspect *11*, 3–7.doi:10.24171/j.phrp.2020.11.1.02

Kim, S.-H., Chang, S.Y., Sung, M., Park, J.H., Bin Kim, H., Lee, H., Choi, J.-P., Choi, W.S., and Min, J.-Y. (2016). Extensive Viable Middle East Respiratory Syndrome (MERS) Coronavirus Contamination in Air and Surrounding Environment in MERS Isolation Wards. Clin. Infect. Dis. *63*, 363–369.doi:10.24171/j.phrp.2020.11.1.02

Koster, A.J., and Klumperman, J. (2003). Electron microscopy in cell biology: integrating structure and function. Nat. Rev. Mol. Cell Biol. *Suppl*, SS6-10.doi: 10.1038/nrm1194

Ng, M.L., Tan, S.H., See, E.E., Ooi, E.E., and Ling, A.E. (2003). Early events of SARS coronavirus infection in vero cells. J. Med. Virol. *71*, 323–331.doi:10.1002/jmv.10499

Oshiro, L.S., Schieble, J.H., and Lennette, E.H. (1971). Electron Microscopic Studies of Coronavirus. Journal of General Virology, *12*, 161–168.doi:10.1099/0022-1317-12-2-161

Park, W.B., Kwon, N.-J., Choe, P.G., Choi, S.-J., Oh, H.S., Lee, S.M., Chong, H., Kim, J.-I., Song, K.-H., Bang, J.H., et al. (2016). Isolation of Middle East Respiratory Syndrome Coronavirus from a Patient of the 2015 Korean Outbreak. J Korean Med Sci *31*, 315–320.doi:10.3346/jkms.2016.31.2.315

Patterson, S., and Macnaughton, M.R. (1982). Replication of Human Respiratory Coronavirus Strain 229E in Human Macrophages. Journal of General Virology, *60*, 307–314.doi:0.1099/0022-1317-60-2-307

Qinfen, Z., Jinming, C., Xiaojun, H., Huanying, Z., Jicheng, H., Ling, F., Kunpeng, L., and Jingqiang, Z. (2004). The life cycle of SARS coronavirus in Vero E6 cells. J. Med. Virol. *73*, 332–337.doi: 10.1002/jmv.20095

Rossen, J.W., Bekker, C.P., Voorhout, W.F., Strous, G.J., van der Ende, A., and Rottier, P.J. (1994). Entry and release of transmissible gastroenteritis coronavirus are restricted to apical surfaces of polarized epithelial cells. J. Virol. *68*, 7966–7973.doi:10.1128/JVI.68.12.7966-7973.1994

Schoeman, D., and Fielding, B.C. (2019). Coronavirus envelope protein: current knowledge. Virology Journal *16*, 69.doi:10.1186/s12985-019-1182-0

Siu, Y.L., Teoh, K.T., Lo, J., Chan, C.M., Kien, F., Escriou, N., Tsao, S.W., Nicholls, J.M., Altmeyer, R., Peiris, J.S.M., et al. (2008). The M, E, and N structural proteins of the severe acute respiratory syndrome coronavirus are required for efficient assembly, trafficking, and release of virus-like particles. J. Virol. *82*, 11318–11330.doi:10.1128/JVI.01052-08

Yuan, X., Yao, Z., Shan, Y., Chen, B., Yang, Z., Wu, J., Zhao, Z., Chen, J., and Cong, Y. (2005). Nucleolar localization of non-structural protein 3b, a protein specifically encoded by the severe acute respiratory syndrome coronavirus. Virus Res. *114*, 70–79.doi:10.1016/j.virusres.2005.06.001

Zhang, Q.-F., Cui, J.-M., Huang, X.-J., Lin, W., Tan, D.-Y., Xu, J.-W., Yang, Y.-F., Zhang, J.-Q., Zhang, X., Li, H., et al. (2003). Morphology and morphogenesis of severe acute respiratory syndrome (SARS)-associated virus. Sheng Wu Hua Xue Yu Sheng Wu Wu Li Xue Bao *35*, 587–591.

Zhu, N., Zhang, D., Wang, W., Li, X., Yang, B., Song, J., Zhao, X., Huang, B., Shi, W., Lu, R., et al. (2020). A Novel Coronavirus from Patients with Pneumonia in China, 2019. New England Journal of Medicine *382*, 727–733.doi:10.1056/NEJMoa2001017

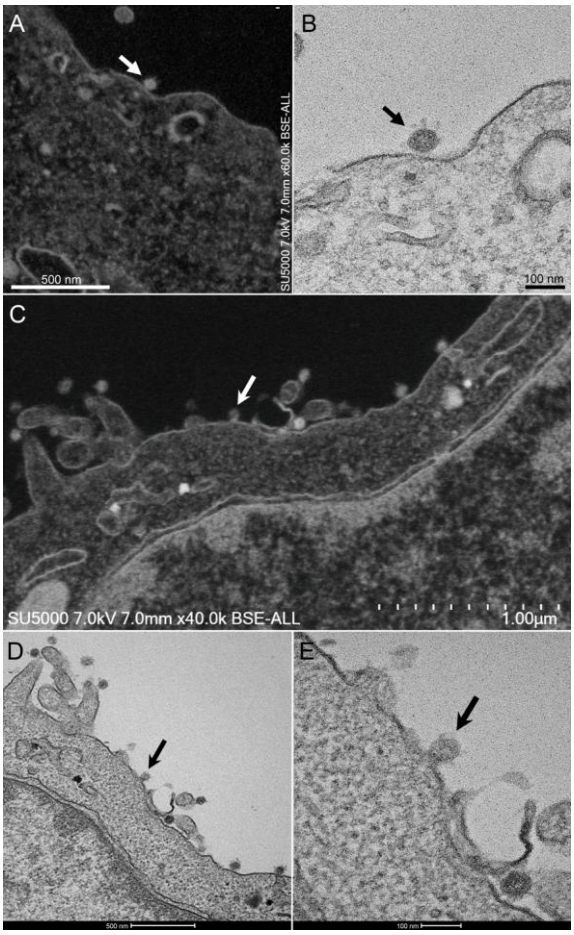

Figure 1: Early-stage SARS-CoV-2 infection(12 hours post-infection) with virus at the periphery of Vero E6 cells.A,B: SEM (A) and TEM (B) views of the same cellular region with a SARS-CoV-2 particle (arrow) attached to the plasma membrane, the corona spikes of which are located between the particle and the cell plasma membrane. C-E: SEM (C) and TEM (D,E) views of the same cellular region showing SARS-CoV-2 virus particles attached to the cell plasma membrane; one particle (arrow in C-E) is glued to the plasma membrane, fusing with the cell plasma membrane.

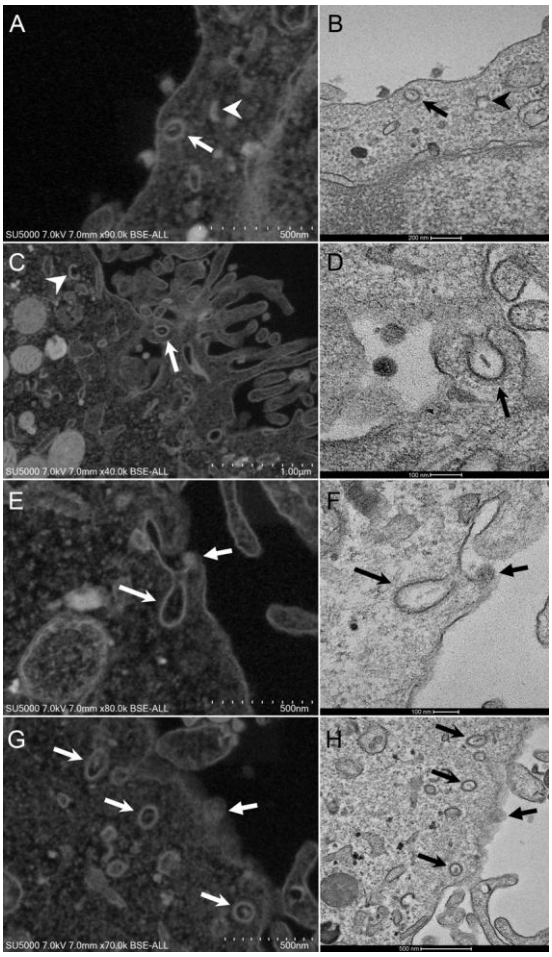

Figure 2: Early-stage SARS-CoV-2 infection (12 hours post-infection) with endocytic vesicles in Vero E6 cells.

A-F: SEM (A,C,E,G) and TEM (B,E,F,H) views of the same cellular regions with clathrin-coated vesicles (arrows) containing rod-like amorphous material. Crescent-like electron-dense structures (arrowhead in A) were often depicted in infected cells cytoplasm. Solid arrows (E-H) point to glued SARS-CoV-2 particles on cells plasma membrane.

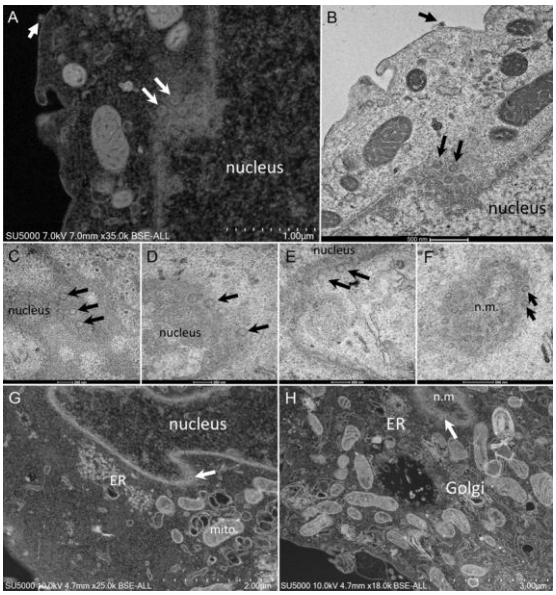

Figure 3: SARS-CoV-2 infected Vero E6 cells at 18-24 hours post-infection. A-H : SEM (A,G,H) and TEM (B-F) images showing numerous virus-like particles (arrows) at nucleus margins (n.m).A-E,G: Images of nuclear membrane budding sites observed in transverse views. F,H:Images of nuclear membrane budding sites in tangential views. SARS-CoV-2 particles can be seen outside the cells at cell plasma membranes (solid arrows in A and B, which correspond to the same cellular region).

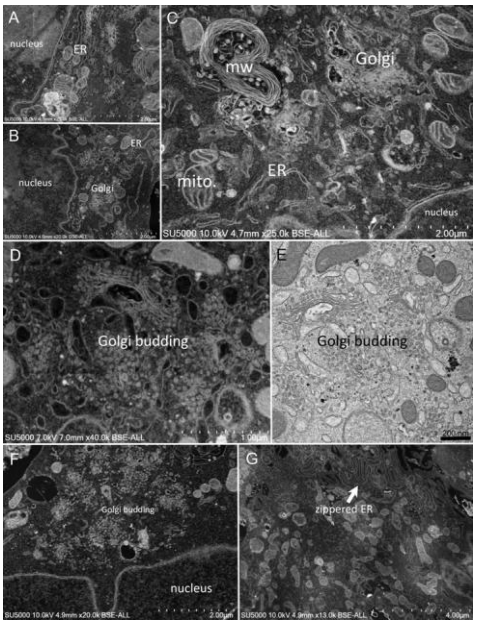

Figure 4: SARS-CoV-2 infected Vero E6 cells at 12-18 hours post-infection. A,B: Thick and distorted endoplasmic reticulum (ER) tubules were observed by SEM at peri-nuclear locations and at the cells periphery. C: SEM view of the extensive enlargement and budding of the ER and Golgi apparatus, as well as a myelin-like membranes whorl (mw) close to the Golgi apparatus and mitochondria (mito.) in the perinuclear region. D,E: SEM (D) and TEM (E) views of the same cell region showing extreme Golgi apparatus budding. F: SEM low-magnification view of Golgi budding between a nucleus and the peripheral plasma membrane. G: SEM image of zippered endoplasmic reticulum (ER) at apical location (arrow). A-F: SEM images.

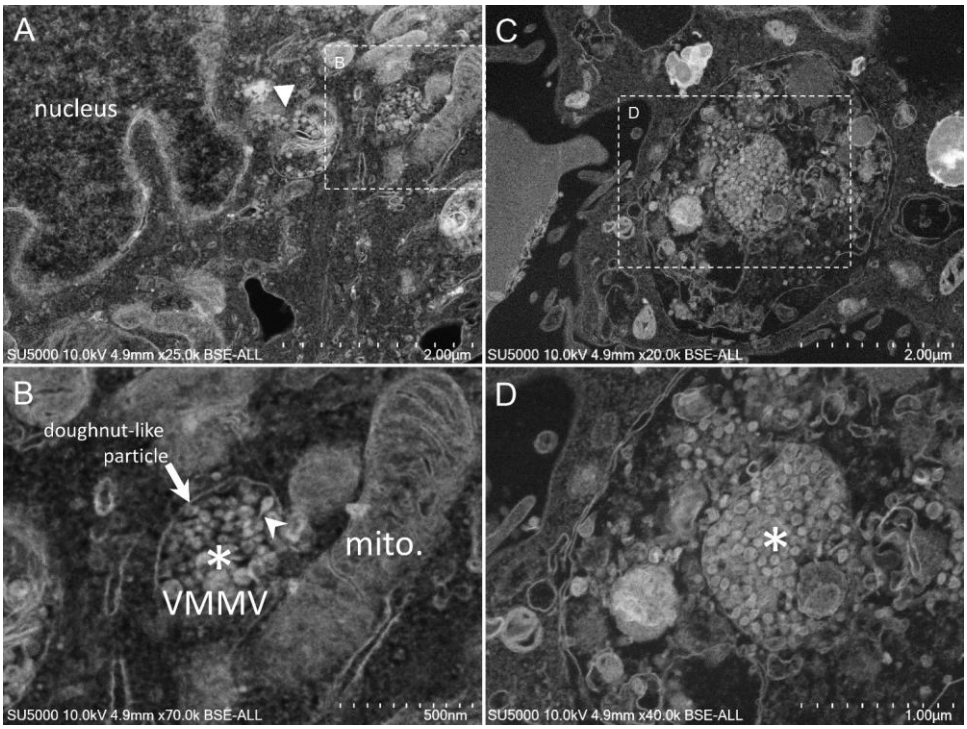

Figure 5: SARS-CoV-2 infected Vero E6 cells at 24-36 hours post-infection. A,B: SEM views of doughnut-like particles (arrow) with a pronounced electron-opaque edge observed at peri-nuclear locations dispersed into the cytoplasm (solid arrowhead), or within vacuoles, which seemed derived from the ER, forming virus morphogenesis matrix vesicae (VMMV). VMMV were observed as opened sacs (asterisk in B), assembling next to the nucleus (A,B). Protrusions of the doughnut-like particles could be observed in the VMMV (arrowhead in B). C,D: VMMV observed as a closed sac (asterisk in D) in a larger vacuole in the cytoplasm. A-D: SEM images.

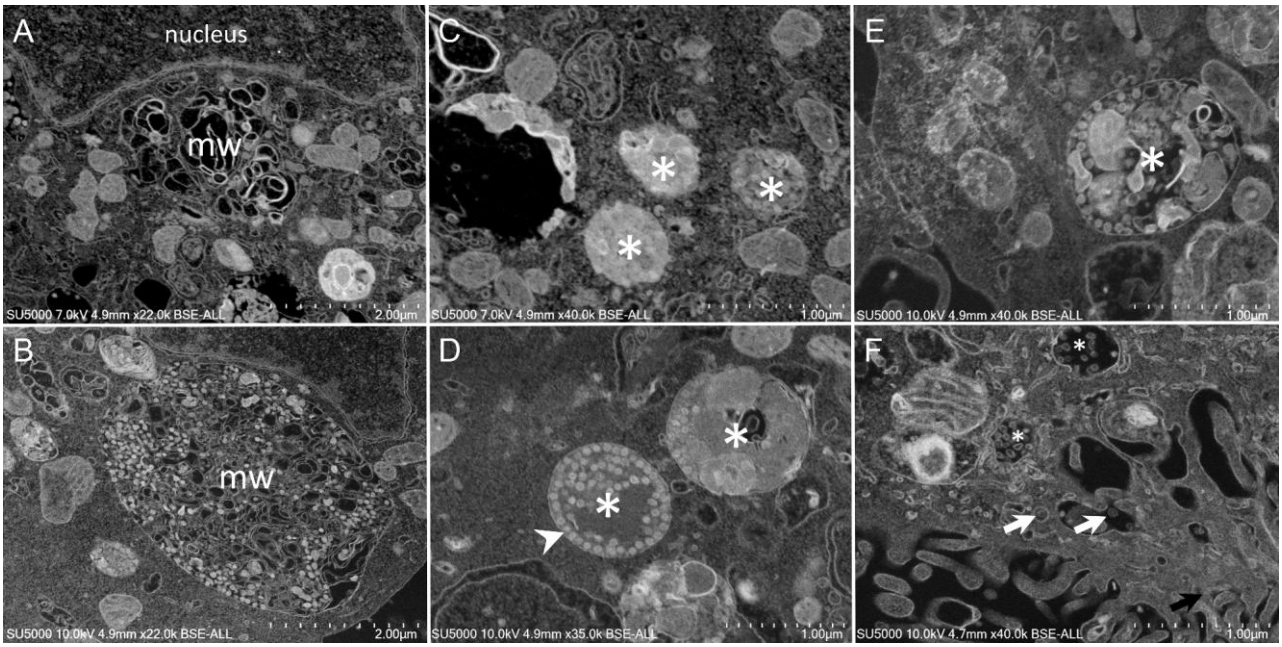

Figure 6: SARS-CoV-2 infected Vero cells at 24-36 hours post-infection A: SEM depiction of an extensive peri-nuclear membrane whorls (mw) network, with larger inner-membranous distances as infection progresses. B: Nascent virions particles (≈75 nm) observed by SEM mixed with membranes whorls in large bags. C,F:SARS-CoV-2-morphogenesis matrix vesicae (asterisk) with different appearances, with nascent particles (≈75 nm) located in more or less large vacuoles, containing more or less electron-dense materials (asterisk). F: translucent VMMV/vacuoles with well-individualized virions particles (white arrows).

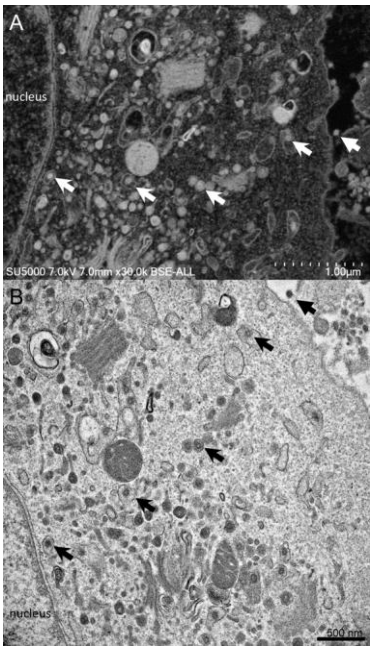

409

410 **Figure 7: Mature SARS-CoV-2 particles in a Vero E6 cell.** A,B: Mature SARS-CoV-2 particles
411 with their corona spikes (arrows) in small cytoplasmic vacuoles between the nucleus and the cell
412 periphery, observed by SEM (A) or TEM (B) in a cell, **12 hours post-infection**. Extracellular
413 particles are also present (Solid arrows).

414

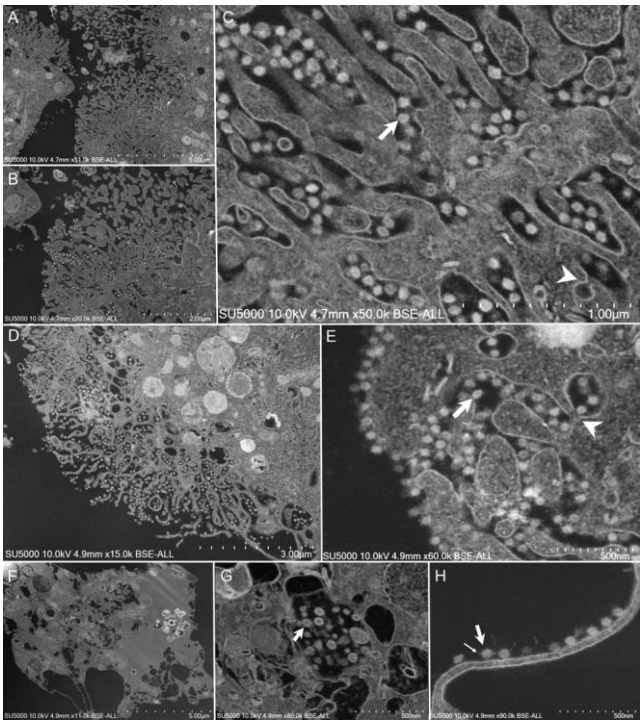

Figure 8: SEM of SARS-CoV-2 mature particles at 24-48 hours post-infection. observed at intra- and extra- cellular locations. A-C:Viral mature particles lying between cellular microvilli. D,E :Virus particles within smooth vesicles at the cell periphery and eventually fused with the cell membrane (arrowhead) to release the virus (arrow). F-G: Viral particles in translucent vacuoles or attached to the plasma membrane of a lysed cell. Small arrow points to a SARS-CoV-2 corona spike.